Preliminary Design of a Multibeam Receiver for the SMA

John D. Garrett, Paul K. Grimes, and Cheuk-Yu Edward Tong

***Abstract*—In these proceedings, we present the preliminary design of a multibeam receiver for the Submillimeter Array (SMA). The design is centered at 345 GHz, which was chosen to coincide with the scientifically important CO(3–2) emission line and its common isotopes. The design presented here has 3 pixels, but we plan to expand the array to 7 pixels in a hexagonal pattern in a future iteration. The array uses sideband separating (2SB) receivers, which greatly improves the mapping speed for narrow emission lines, when compared to equivalent double sideband receivers. Compared to the wSMA's planned high-band dual-polarization receiver, a 7-pixel 2SB multibeam system should provide $\sim$7 times faster mapping speed. This would allow for large-scale mapping of molecular emission lines in the Milky Way and nearby galaxies with very high angular resolution.**

***Index Terms*—multibeam receivers, focal plane arrays, SIS mixers, superconducting detectors, submillimeter-wave astronomy**

I. Introduction

THE Submillimeter Array (SMA) is an eight-element radio interferometer located near the summit of Mauna Kea, Hawaii, that operates from 180-420 GHz. It is currently undergoing a large-scale upgrade to improve the noise performance and increase the instantaneous bandwidth of its receivers [1], [2], [3]. Through the wideband SMA (wSMA) upgrade, the SMA antennas will be refitted with new cryostats housing new receiver cartridges. These receivers will operate over two bands: a low-band from 210–270 GHz and a high-band from 280–360 GHz. Among other benefits, the new receivers will improve the SMA's sensitivity to continuum sources and increase the number of emission lines that can be observed simultaneously. Since the new wSMA cryostat will be smaller than the current SMA cryostat, there will soon be enough room to host guest receivers inside the receiver cabins, allowing for the ability to test new receiver designs with the wSMA, including new multibeam systems.

Multibeam receivers (also called focal plane arrays) have the potential to increase the mapping speed of a telescope by a factor equal to the number of pixels N within the array (when compared to an equivalent single-beam design). However, the mapping speed is also inversely proportional to the system noise temperature $T_{\rm sys}$ squared:

$$\text{mapping speed} \propto \frac{N}{T_{\rm sys}^2} \tag{1}$$

John D. Garrett, Paul K. Grimes and Cheuk-Yu Edward Tong are with the Center for Astrophysics | Harvard & Smithsonian, Cambridge, MA 02138, USA (e-mail: john.garrett@cfa.harvard.edu; pgrimes@cfa.harvard.edu; etong@cfa.harvard.edu).

Therefore, any increase in the system noise temperature can quickly negate the speed improvement afforded by the array. This means that any multibeam system must add additional pixels without compromising on the state-of-the-art noise performance of modern single-beam systems. Additional challenges include efficiently coupling each pixel to the main dish, managing the added mechanical/electrical complexity, dividing and injecting the local-oscillator (LO) signal without interfering with the astronomical signal path, and processing the additional intermediate frequency (IF) signals. (Comprehensive discussions of focal plane arrays can found in [4], [5], [6].)

Overall, a multibeam receiver on the wSMA would allow for wide-field mapping of molecular emission lines at high angular resolution. The improved mapping capability would be beneficial for a variety of observations, including the study of star formation in the Milky Way and nearby galaxies. It would also be the first multibeam system on an interferometer, taking advantage of the wSMA correlator system. As such, it would be able to act as a pathfinder for future multibeam systems on other large submillimeter-wave interferometers, such as the Atacama Large Millimeter/Submillimeter Array (ALMA) and the Northern Extended Millimeter Array (NOEMA). Due to its modest size and the ability to host guest receivers, the wSMA provides an excellent environment to test and develop new multibeam receivers for submillimeter wave interferometers.

In this work, we discuss the requirements for a multibeam receiver on the wSMA in Sec. II, investigate the potential mapping speed improvement in Sec. III, and present a preliminary multibeam system in Sec. IV. Sec. V concludes this study.

II. Design Considerations

There are several design considerations, specific to the wSMA, which influence the optimal multibeam receiver architecture. First, the maximum size of an array on the wSMA is limited by the size of the Nasymth tubes within the antennas. A low-band array ($\nu \sim 230$ GHz) would be limited to $\sim$3 pixels in a triangular pattern and a high-band array ($\nu \sim 345$ GHz) would be limited to 7 pixels in a hexagonal pattern. Since both bands target important molecular emission lines (e.g., the CO(2–1) and the CO(3–2) transitions, respectively) and both have good atmospheric transmission at the SMA site, a 7-pixel array centered at 345 GHz presents a greater potential mapping speed improvement.

Secondly, the array will use a similar backend to the wSMA. Assuming a total processed IF bandwidth of 64 GHz, this limits the IF bandwidth to $\sim$4.6 GHz per pixel for a 7-pixel

2SB receiver or ∼9.2 GHz per pixel for a 7-pixel DSB array. Since the total processed IF bandwidth will be identical to the wSMA's single-beam receivers, the primary advantage of the array will be mapping narrow emission lines (the continuum mapping speed will be similar to the wSMA). Therefore, image sideband rejection would help to lower the system noise temperature and further increase the mapping speed. This could be accomplished by using a sideband separating (2SB) mixing scheme, or by terminating the image sideband in a reactive or cryogenic load (e.g., using a narrow bandpass filter to only pass the desired signal).

III. Mapping Speed Improvement

In this section, we compare the mapping speed of different multibeam receiver architectures: double sideband (DSB) receivers and single sideband (SSB) receivers. Based on Eqn. 1, the mapping speed of two different multibeam receivers can be compared using:

$$\Gamma_{2,1} = \frac{N_2}{N_1}\left(\frac{T_{\rm sys,1}}{T_{\rm sys,2}}\right)^2 \tag{2}$$

where $T_{\rm sys}$ is the SSB system noise temperature[1] (including receiver and atmospheric noise) and N is the number of pixels in the array ($N = 1$ for a single-beam receiver).

For a ground based DSB receiver, the SSB system noise temperature is [7], [8]:

$$T_{\rm sys}^{\rm DSB} = \frac{2\left(T_{\rm rx}^{\rm DSB} + T_{\rm sky}\right)}{e^{-\tau}} \tag{3}$$

where $T_{\rm rx}^{\rm DSB}$ is the DSB receiver noise temperature[2], $T_{\rm sky}$ is the atmospheric brightness temperature, and $e^{-\tau}$ is the atmospheric transmission. Likewise, for a SSB receiver, the SSB system noise temperature is:

$$T_{\rm sys}^{\rm SSB} = \frac{2\,T_{\rm rx}^{\rm DSB} + T_{\rm sky}\,(1 + 1/R_{\rm sb})}{e^{-\tau}} \tag{4}$$

where $R_{\rm sb} = G_s/G_i$ is the sideband ratio, i.e., the ratio of the signal sideband gain G_s to the image sideband gain G_i. For an ideal SSB receiver, $R_{\rm sb} \to \infty$ and Eqn. 4 reduces to:

$$T_{\rm sys}^{\rm SSB} = \frac{2\,T_{\rm rx}^{\rm DSB} + T_{\rm sky}}{e^{-\tau}} \tag{5}$$

Note that Eqns. 3–5 ignore several noise contributions, including the cosmic microwave background and spillover effects. The main beam efficiency and the loss of the sideband separation scheme are also ignored. More detailed $T_{\rm sys}$ calculations can be found in [8], [9].

Using Eqns. 3–5, the system noise temperature is plotted in Fig. 1 for SSB and DSB receivers. For this plot, we assumed $T_{\rm rx}^{\rm DSB} = 55$ K, which is the target value for the wSMA's single-beam high-band receiver [1], and we calculated $e^{-\tau}$ and $T_{\rm sky}$ using the am atmospheric model [10] with a precipitable water vapor of 1.86 mm (the median value at the SMA site).

[1]In this report, we always use the SSB system noise temperature, unless specified otherwise. The SSB $T_{\rm sys}$ is the most important figure-of-merit for observing narrow emission lines, which are only present in one sideband.

[2]$T_{\rm rx}^{\rm DSB}$ is the noise temperature value that is normally measured in the lab via the Y-factor technique (since the test signal is present in both sidebands.)

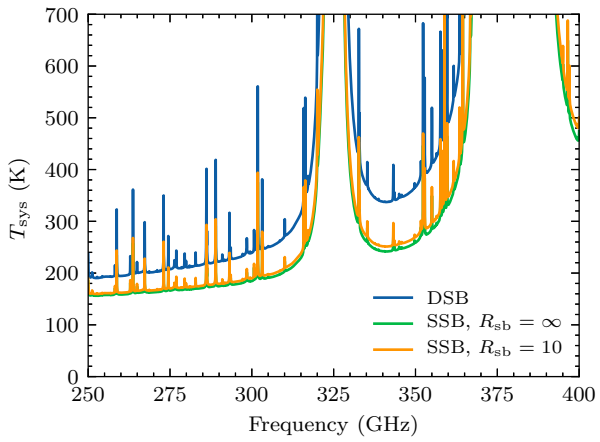

Fig. 1. Estimated SSB system noise temperature ($T_{\rm sys}$) of DSB and SSB receivers (Eqns. 3–5). For this plot, we assumed $T_{\rm rx}^{\rm DSB}$=55 K and a precipitable water vapor of 1.86 mm, which is the median value at the SMA site. The atmospheric properties were calculated using the am atmospheric model [10].

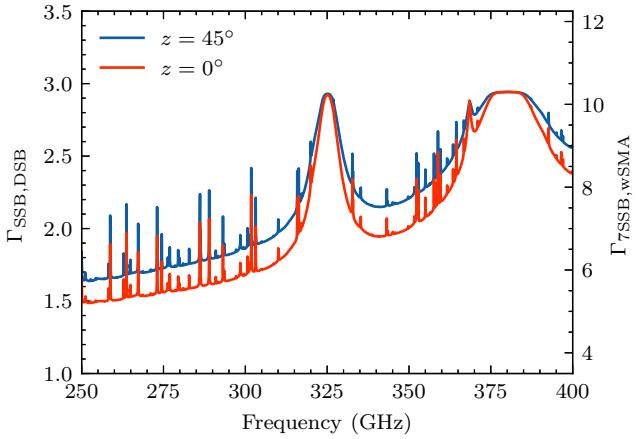

Fig. 2. Mapping speed ratio of a SSB receiver compared to a DSB receiver (left y-axis; calculated using Eqn. 2). This is plotted for two different zenith angles: z=0° and z=45°. The right y-axis compares a 7 pixel SSB multibeam receiver to the wSMA's single-beam DSB receiver.

As we can see, the ideal SSB receiver ($R_{\rm sb} \to \infty$) has a significantly lower $T_{\rm sys}$ value than the DSB receiver because it is able to remove the atmospheric noise contribution from the image sideband. This reduces the overall $T_{\rm sys}$ value by ∼29% at 345 GHz. Even with a modest sideband ratio of $R_{\rm sb} = 10$, the atmospheric noise in the image sideband is reduced by 90% and $T_{\rm sys}$ is reduced by ∼26%.

Based on Eqn. 2, lower system noise temperatures result in faster mapping speeds. In Fig. 2, the mapping speed of a SSB receiver is compared to a DSB receiver. As we can see, at 345 GHz, the SSB receiver has a mapping speed that is approximately twice as fast as the DSB receiver. Furthermore, the SSB receiver provides an even greater mapping speed improvement as the atmospheric transmission worsens (e.g., when there is a higher precipitable water vapor or a larger zenith angle).

The downside is that SSB receivers are much more complicated than DSB receivers. For example, image rejec-

tion can be accomplished by a tuneable waveguide backshort (e.g., HERA [11]), a Mach-Zehnder interferometer (e.g., HARP [12]), a Martin-Puplett interferometer (e.g., CHAMP+ [13]) or a cryogenic waveguide bandpass filter. These image rejection schemes generally have limited IF bandwidth and are very cumbersome. Another option is to separate the signal and image sidebands using a 2SB receiver. This has the added advantage of recovering both the upper and lower sidebands; however, it essentially doubles the complexity of the receiver. For example, a 2SB receiver requires a 90° hybrid for the RF signal, a power divider for the LO signal, two RF/LO diplexers and two SIS mixers per pixel. For our purposes, the added complexity of the 2SB receiver architecture is acceptable because our array will be a relatively modest 7 pixels.

We can rewrite Eqn. 2 to calculate the mapping speed improvement of a 7-pixel 2SB mutlibeam receiver when compared to the wSMA single-beam receiver[3]:

$$\Gamma_{7\mathrm{SSB,wSMA}} = \frac{7}{2}\left(\frac{T_{\mathrm{sys}}^{\mathrm{DSB}}}{T_{\mathrm{sys}}^{\mathrm{SSB}}}\right)^2 \tag{6}$$

This value is plotted in Fig. 2 using the y-axis on the right-hand side. As we can see, a 7-pixel 2SB multibeam receiver should be able to map the CO(3–2) emission line at 345.8 GHz approximately 7 times faster than the wSMA single-beam receiver.

IV. Preliminary Design of the Multibeam Receiver

The preliminary design of the multibeam receiver is shown in Figs. 3 and 4. The construction is similar to the array proposed for the Greenland Telescope [14], except that this new design has been expanded from DSB receivers to 2SB receivers. The design uses a combination of split-block waveguides (with the split in the E-plane of the waveguide) and stacked waveguide plates (where the direction of propagation is normal to the split plane). The design shown in Figs. 3 and 4 only has 3 pixels, but we plan to expand this array to 7 pixels in the near future, with the pixels arranged in a hexagonal pattern.

The RF (astronomical) signals enter the array block through the feed horns shown at the top of Fig. 4. RF quadrature hybrids then divide each RF signal into two separate waveguides with a 90° relative phase shift, which is necessary for sideband separation[4]. The LO signal enters from the side of the mixer block (Fig. 5). It is evenly divided into six waveguides using cascaded E-plane power splitters (0° relative phase shift), and then each LO waveguide is diverted 90° using H-plane waveguide bends to be parallel to the RF waveguides. Note that there are two LO waveguides per pixel. The RF and LO signals are then diplexed using silicon-mounted cross-guide couplers [15], and each RF+LO signal is coupled to an SIS mixer device. Finally, the two down-converted IF signals from each pixel are combined using another 90° hybrid to recover the upper and lower sidebands (not shown). It is also possible implement this step in the digital backend of the telescope.

This multibeam receiver will be designed to cover the atmospheric window centered at $\sim$345 GHz (seen in Figs. 1 and 2). Since most of the important molecular emission lines are situated between 329 GHz and 355 GHz, the multibeam receiver can get away with a narrower RF bandwidth than the wSMA's high-band receiver, without compromising on the utility of the receiver. For example, the CO(3–2), ^{13}CO(3–2)

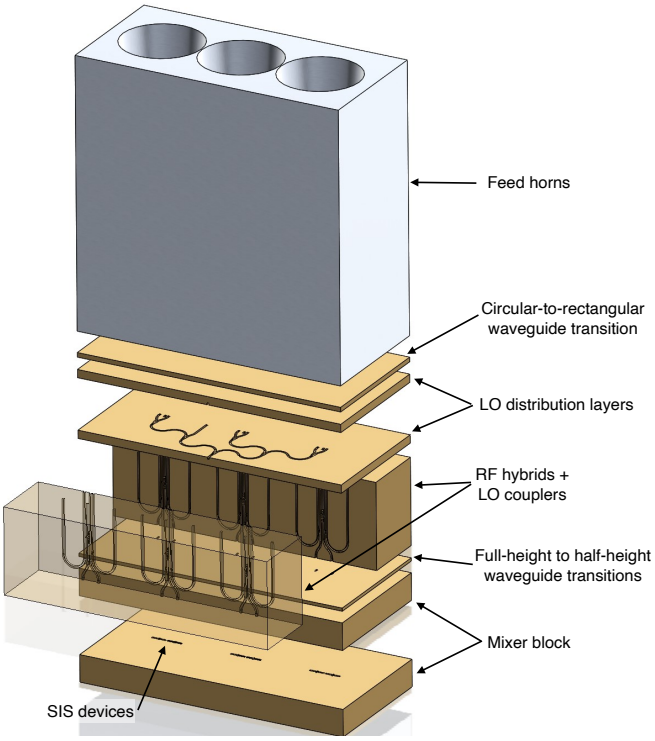

Fig. 3. Exploded view of the preliminary 3-pixel 2SB multibeam receiver. Most of the waveguide components are made from stacked waveguide plates, where the direction of propagation is normal to the split plane. The RF hybrids and LO direction couplers are made from a single split-block waveguide, where the split is in the E-plane of the waveguide.

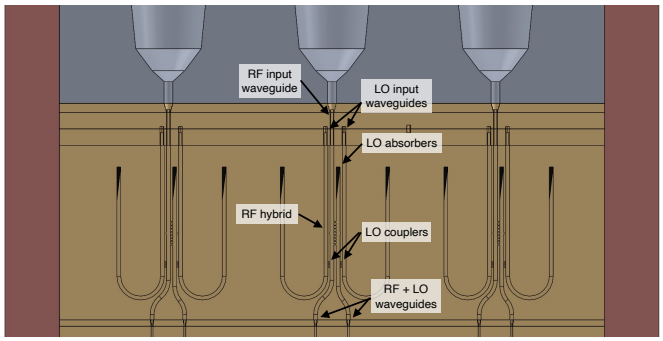

Fig. 4. Cross-section of the 3-pixel 2SB multibeam receiver. Each RF signal first passes through an RF hybrid, which divides the RF signal in two with a 90° relative phase difference. The LO signals are diplexed with the RF signals using silicon-mounted cross-guide couplers (the same coupler that is used by the wSMA's single-beam receivers [15]).

[3]Note that the wSMA single-beam receivers are dual-polarization. Assuming that polarization data is not important, $N_{\mathrm{wSMA}} = 2$.

[4]Alternatively, it is possible to divide the RF signals using in-phase power splitters and divide the LO signals using 90° RF hybrids. This can allow for wider RF bandwidth, but in-phase power splitters generally suffer from poor isolation and poor return loss, which in turn degrades R_{sb} and T_{sys}.

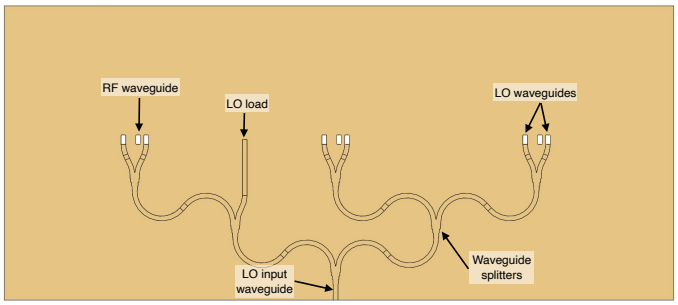

Fig. 5. Cross-section of the local-oscillator (LO) distribution layer. The LO signal enters from the bottom of this figure and then it is divided in six using cascaded E-plane power dividers. The LO waveguides are then diverted downwards using H-plane waveguide bends to be in parallel with the RF waveguides. There are two LO waveguides per RF waveguides. Note that the LO power dividers require excellent isolation to minimize cross-talk between the RF waveguides.

and $C^{18}O$(3–2) transitions occur at 345.8 GHz, 330.6 GHz and 329.3 GHz, respectively. Furthermore, since the target objects have to have relatively large angular diameters for the array to be beneficial, the array will only be used on low-redshift objects ($z \sim 0$), meaning that we do not need to consider redshifted emission lines. Therefore, we can optimize the performance of the array from ∼329–356 GHz to achieve the best possible noise temperature.

To achieve a high $R_{\rm sb}$ value, the array block will require careful fabrication, especially for the RF hybrids and the LO power dividers. Any machining errors could result in amplitude and phase imbalances that will lower the $R_{\rm sb}$ value and thereby cause a higher noise temperature.

Finally, note that these are preliminary drawings, meaning that many important features are missing from the CAD drawings in Figs. 3–5, e.g., coaxial cables, magnetic coils, etc. We are also considering several design modifications including using silicon-mounted RF hybrids to facilitate fabrication, using permanent magnets to suppress the Josephson currents and reduce the number of DC wires, and using integrated SiGe low noise amplifiers (LNAs) to minimize the heat load of the array.

V. Conclusion

We have presented the preliminary design of a multibeam receiver for the SMA. Once the wSMA upgrade is complete, this receiver could be mounted in the guest cryostat inside the wSMA receiver cabin. The proposed 7-pixel sideband separating receiver has the potential to increase the mapping speed of the wSMA by a factor of ∼7. This would allow for large-scale surveys with the wSMA of molecular emission lines in the Milky Way and nearby galaxies.

References

[1] P. Grimes, E. Tong, S. Paine, L. Zeng, and R. Blundell, "Introducing the wSMA: A Major Upgrade to the SMA Receiver Systems," *Submillimeter Array Newsletter*, vol. 23, pp. 17–19, Jan. 2017.

[2] R. Rao, P. Grimes, E. Tong, and D. Wilner, "Science with the Upgraded ultra-wideband Submillimeter Array (wSMA) in the Next Decade," in *2019 URSI Asia-Pacific Radio Science Conference (AP-RASC)*, New Delhi, India, Mar. 2019.

[3] P. Grimes, R. Blundell, S. Paine, E. Tong, and L. Zeng, "Receivers for the wideband Submillimeter Array," in *Proceedings of the 31st International Symposium on Space Terahertz Technology (ISSTT)*, Tempe, AZ, Mar. 2020.

[4] C. E. Groppi and J. H. Kawamura, "Coherent Detector Arrays for Terahertz Astrophysics Applications," *IEEE Transactions on Terahertz Science and Technology*, vol. 1, no. 1, pp. 85–96, Sep. 2011.

[5] P. F. Goldsmith, "Sub-Millimeter Heterodyne Focal-Plane Arrays for High-Resolution Astronomical Spectroscopy," *The Radio Science Bulletin*, vol. 2017, no. 362, pp. 53–73, Sep. 2017.

[6] J. D. Garrett, "A 230 GHz Focal Plane Array Using a Wide IF Bandwidth SIS Receiver," DPhil dissertation, University of Oxford, 2018.

[7] C. Groppi, A. Baryshev, U. Graf, M. Wiedner, P. Klaassen, and T. Mroczkowski, "First Generation Heterodyne Instrumentation Concepts for the Atacama Large Aperture Submillimeter Telescope," in *Proceedings of the 30th International Symposium on Space Terahertz Technology (ISSTT)*, Gothenburg, Sweden, Apr. 2019.

[8] J. W. Lamb, "SSB vs . DSB for Submillimeter Receivers," *ALMA Memo 301*, Apr. 2000.

[9] A. Remijan, A. Biggs, P. Cortes, B. Dent, J. Di Francesco, E. Fomalont, A. Hales, S. Kameno, B. Mason, N. Philips, K. Saini, F. Stoehr, B. Vila Vilaro, and E. Villard, "ALMA Technical Handbook, ALMA Doc. 8.3, ver. 1.0," *ALMA partnership*, 2020.

[10] S. Paine, "The am atmospheric model," 2019. [Online]. Available: https://zenodo.org/record/3406483

[11] K.-F. Schuster, C. Boucher, W. Brunswig, M. Carter, J.-Y. Chenu, B. Foullieux, A. Greve, D. John, B. Lazareff, S. Navarro, A. Perrigouard, J.-L. Pollet, A. Sievers, C. Thum, and H. Wiesemeyer, "A 230 GHz heterodyne receiver array for the IRAM 30 m telescope," *Astronomy & Astrophysics*, vol. 423, no. 3, pp. 1171–1177, Sep. 2004.

[12] J. V. Buckle, R. E. Hills, H. Smith, W. R. F. Dent, G. Bell, E. I. Curtis, R. Dace, H. Gibson, S. F. Graves, J. Leech, J. S. Richer, R. Williamson, S. Withington, G. Yassin, R. Bennett, P. Hastings, I. Laidlaw, J. F. Lightfoot, T. Burgess, P. E. Dewdney, G. Hovey, a. G. Willis, R. Redman, B. Wooff, D. S. Berry, B. Cavanagh, G. R. Davis, J. Dempsey, P. Friberg, T. Jenness, R. Kackley, N. P. Rees, R. Tilanus, C. Walther, W. Zwart, T. M. Klapwijk, M. Kroug, and T. Zijlstra, "HARP/ACSIS: a submillimetre spectral imaging system on the James Clerk Maxwell Telescope," *Monthly Notices of the Royal Astronomical Society*, vol. 399, no. 2, pp. 1026–1043, Oct. 2009.

[13] C. Kasemann, S. Heyminck, A. Bell, A. Belloche, C. Castenholz, R. Gusten, H. Hafok, A. Henseler, S. Hochgurtel, T. Klein, I. Kramer, A. Korn, K. Meyer, D. Muders, F. Pacek, F. Schafer, G. Schneider, G. Wieching, H.-J. Wunsch, A. Baryshev, R. Hesper, T. Zijlstra, C. Lodewijk, and T. Klapwijk, "CHAMP+: A Powerful Submm Heterodyne Array," in *Proceedings of the 19th International Symposium on Space Terahterz Technology (ISSTT)*, Groningen, Netherlands, Apr. 2008, pp. 166–172.

[14] P. K. Grimes, K. Asada, R. Blundell, R. Burgos, H.-H. Chang, M. T. Chen, D. Goldie, C. Groppi, C. C. Han, P. T. P. Ho, Y. D. Huang, M. Inoue, D. Kubo, P. Koch, J. Leech, E. de Lera Acedo, P. Martin-Cocher, H. Nishioka, M. Nakamura, S. Matsushita, S. N. Paine, N. Patel, P. Raffin, W. Snow, T. K. Sridharan, R. Srinivasan, C. N. Thomas, C.-Y. E. Tong, M.-J. Wang, C. Wheeler, S. Withington, G. Yassin, and L.-Z. Zeng, "Instrumentation for single-dish observations with The Greenland Telescope," in *SPIE Astronomical Telescopes + Instrumentation*, vol. 9153, Jul. 2014, p. 91531V.

[15] L. Zeng, E. Tong, and P. Grimes, "Waveguide Components for wSMA Frontends," in *Proceedings of the 31st International Symposium on Space Terahertz Technology (ISSTT)*, Tempe, AZ, Mar. 2020.